Annals of Biomedical Engineering (2024) 52:2496–2508
https://doi.org/10.1007/s10439-024-03538-5

BMES BIOMEDICAL ENGINEERING SOCIETY

ORIGINAL ARTICLE

Effect of Tear Size and Location on Supraspinatus Tendon Strain During Activities of Daily Living and Physiotherapy

Mason Garcia[1,2] · Gabriel Landi[1] · Bailee Covan[1] · Daniela Caro[1] · Mohammad Khak[1,3] · Ahmad Hedayatzadeh Razavi[1,2] · Joseph P. DeAngelis[1,3] · Arun J. Ramappa[1,3] · Ara Nazarian[1,2,3,4]

Received: 7 October 2023 / Accepted: 6 May 2024 / Published online: 20 July 2024
© The Author(s) under exclusive licence to Biomedical Engineering Society 2024

Abstract

The supraspinatus tendon plays a crucial role in shoulder abduction, making it one of the common structures affected by injury. Clinically, crescent-shaped tears are the most commonly seen tear shape. By developing six specimen-specific, three-dimensional, supraspinatus-infraspinatus finite element model with heterogeneous material properties, this study aimed to examine the changes in tissue deformation (maximum principal strain) of the supraspinatus tendon due to specimen-specific material properties and rotator cuff tear size. FE models with small- and medium-sized full-thickness crescent-shaped tears were subjected to loads seen during activities of daily living and physiotherapy. Six fresh-frozen cadaveric shoulders were dissected to mechanically test the supraspinatus tendon and develop and validate FE models that can be used to assess changes in strain due to small (< 1 cm, equivalent to 20-30% of the tendon width) and medium-sized (1–3 cm, equivalent to 40–50% of the tendon width) tears that are located in the middle and posterior regions of the supraspinatus tendon. FE predictions of maximum principal strain at the tear tips were examined to determine whether failure strain was reached during activities of daily living (drinking and brushing teeth) and physiotherapy exercises (prone abduction and external rotation at 90° abduction). No significant differences were observed between the middle and posterior tear failure loads for small- and medium-sized tears. For prone abduction, there was a potential risk for tear progression (exceeded failure strain) for medium-sized tears in the supraspinatus tendon's middle and posterior regions. For external rotation at 90° abduction, one model with a middle tear and two with posterior tears experienced failure. For all daily activity loads, the strain never exceeded the failure strain. Our three-dimensional supraspinatus-infraspinatus FE model shows that small tears appear unlikely to progress based on the regional strain response; however, medium-sized tears are at higher risk during more strenuous physiotherapy exercises. Furthermore, differences in patient-specific tendon material properties are important in determining whether the tear will progress. Therefore, patient-specific management plans based on tear size may be beneficial to improve clinical outcomes.

Keywords Supraspinatus · Rotator cuff tear · Rotator cuff injury · Finite element analysis · Principal strain · Tear progression

Introduction

Partial and full-thickness rotator cuff (RC) tears have been found in 64% of patients reporting unilateral shoulder pain, correlating positively with age [1]. Despite its

Associate Editor Joel Stitzel oversaw the review of this article.

Joseph P. DeAngelis, Arun J. Ramappa, and Ara Nazarian have contributed equally as senior authors.

✉ Ara Nazarian
anazaria@bidmc.harvard.edu

[1] Musculoskeletal Translational Innovation Initiative, Beth Israel Deaconess Medical Center, Harvard Medical School, 330 Brookline Avenue, RN123, Boston, MA 02115, USA

[2] Mechanical Engineering Department, Boston University, Boston, MA, USA

[3] Carl J. Shapiro Department of Orthopaedic Surgery, Beth Israel Deaconess Medical Center, Harvard Medical School, Boston, MA, USA

[4] Department of Orthopaedic Surgery, Yerevan State Medical University, Yerevan, Armenia

high prevalence, the mechanism of RC tear progression remains unclear, leaving physicians with few means of predicting how a patient's pain, shoulder mobility, and tear size will change over time [2–5]. Consequently, 49% of patients undergoing nonsurgical treatment experience increases in tear sizes between the two- and three-year follow-up periods [4]. Furthermore, 18% of patients presenting with small- and medium-sized RC tears are not relieved of symptoms within the first year [6].

The RC comprises four muscle-tendon subunits that provide stability and mobility to the shoulder joint: the subscapularis, supraspinatus, infraspinatus, and teres minor [7]. The supraspinatus plays an important role in dynamically stabilizing the glenohumeral (GH) joint. It is the main muscle-tendon unit during abduction [8–12], and the most commonly affected tendon by injury and degeneration [13–17]. While the supraspinatus is the primary abductor of the RC, it has also been shown that during the abduction, the load-sharing interaction from the infraspinatus contributes to increased strain on the supraspinatus [18–20]. This, in addition to hypo-vascularity, repetitive micro-trauma, and internal impingement, can decrease the tensile strength of the tendon and lead to tears [21].

It has been longstanding and widely accepted that degenerative RC tears initiate in the anterior region of the supraspinatus tendon, usually beginning as partial-thickness tears on the articular surface and eventually progressing posteriorly and into full-thickness tears [22–25]. Clinically, the most common type of RC tears seen are crescent-shaped tears, with similar anterior-posterior and medial-lateral tear dimensions [26]. Recent literature has suggested that RC tears originate more posteriorly than previously thought. Kim et al. found that 96% of the tears they studied were located 13-16 mm posterior from the biceps tendon [27], lying within the rotator crescent in the posterior region of the supraspinatus tendon. Jeong et al. conducted a similar study, where they reported the most common tear origin location was 9.5-10 mm posterior to the biceps tendon lying in the middle region of the supraspinatus tendon [28]. Furthermore, the supraspinatus tendon has highly heterogeneous mechanical properties. It has been shown that the anterior region of the supraspinatus tendon is mechanically the strongest, with the highest modulus, failure load, and failure stress, which all decrease posteriorly [29]. Samples taken near the tendon-bone insertion show that modulus is greater on the bursal surface than on the articular surface [30], and that the tendon is stiffer at the tendon-bone insertion than at the musculotendinous junction [31]. Due to spatial heterogeneity, tear location may be important when evaluating which tears are at a higher risk of progress.

Finite element (FE) models have been widely implemented in biomechanical research because they provide otherwise immeasurable data on internal mechanical environments without the added cost, time, and ethical considerations of in vivo experiments. Recently, studies have adopted patient-specific geometry and material properties to shed light on tissue degeneration [32], tear progression [33,34], and repair [35]. However, further improvements can be made in characterizing the material properties of the supraspinatus tendon by quantifying collagen fiber orientation and capturing the full spatial heterogeneity of the material properties of the supraspinatus tendon. Consideration of collagen fiber misalignment due to degeneration or injury is especially relevant to the supraspinatus tendon, as it displays more variation in collagen fiber orientation than other tendons [36–38], suggesting that the supraspinatus tendon may not be transversely isotropic, as previously modeled [32,33,39]. Accurate simulation of tissue geometry, material properties, and boundary conditions is critical to creating FE models worthy of consideration in clinical applications [40].

Therefore, this study seeks to develop a hyper-elastic FE model of the supraspinatus and infraspinatus tendon unit using collagen-informed material properties that mimic the spatial variation in the mechanical response to loading. Following validation with cadaveric experimental data [41], we aim to examine tendon strain with small- and medium-sized full-thickness tears of the supraspinatus tendon originating in the middle and posterior regions. Using loading conditions found in activities of daily living and physiotherapy regimens, we can better understand how RC tears affect the mechanical response of the supraspinatus tendon, allowing for more informed clinical decision-making. We hypothesize that tears in the middle region will be more likely than posterior-sided tears to progress, experiencing lower failure loads and higher strains during daily living and physical therapy loading conditions.

Materials and Methods

Specimen Preparation

Six fresh-frozen intact cadaveric shoulders (Medcure, Inc., Providence, RI, USA) from six female donors with a mean age of 65 ± 9 were used for material testing. The skin and all soft tissue were removed, leaving the supraspinatus muscle-tendon unit. The condition of the tendons was then evaluated to identify gross level degeneration (tears or calcific lesions)—none were found, indicating an intact specimen. The supraspinatus was then sharply dissected from its insertion. Due to the supraspinatus tendon's heterogeneity, the tendon was sectioned to account for region-specific material properties. The tendon width was measured and sectioned into equal thirds, creating anterior, middle, and posterior strips. Each strip was further sectioned by

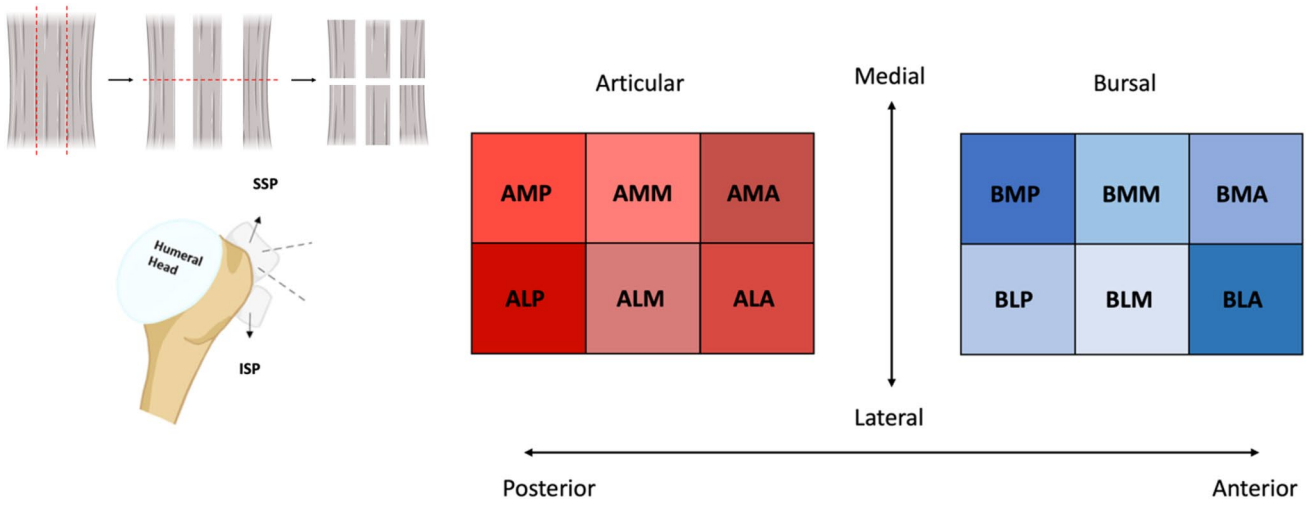

Fig. 1 Example of supraspinatus tendon sectioning (red lines represent cuts) and the final regions of the tendon with corresponding names. The first letter represents the articular (**A**) or bursal (**B**) side, the second letter represents the medial (M) or lateral (L) side, and the third letter represents the anterior (A), middle (M), or posterior (P) regions

cutting it in half in the medial to the lateral plane (Fig. 1). To separate the articular and bursal sides, each sample was embedded in Optimal Cutting Temperature (O.C.T) compound (Tissue-Tek, Sakura FineTek, Torrance, CA, USA), and pre-sectioned using a cryostat (Leica CM3050S, Leica Biosystems, Danvers, MA, USA) until the tendon surface was flush with the OCT. Then the surface layer, and any extra soft tissue, was removed by sectioning off 250 µm. Lastly a 1-mm section was cut from the surface to obtain the articular side (inner surface). The sample was then flipped over and the process was then repeated to obtain the bursal side (outer surface). Finally, after removing the samples from the OCT, the samples were trimmed to fit into out materials testing machines.

Overall, this yielded 12 regions per tendon (Fig. 1). All samples were trimmed to approximately 10 mm (ML length) × 5 mm (AP length) × 1 mm (thickness). For simplicity, all regions were abbreviated with three-letter codes representing their anatomical location within the supraspinatus tendon. The first letter represents the articular (A) or bursal (B) side, the second letter represents the medial (M) or lateral (L) side, and the third letter represents the anterior (A), middle (M), or posterior (P) regions (Fig. 1).

Material Testing

To appropriately capture and characterize the heterogeneity and mechanical response of the supraspinatus tendon, uniaxial tensile testing was used to determine the stress-strain response of each region. Each sample underwent uniaxial tensile loading with a uniaxial tensile testing system specific for small soft tissue (UniVert, CellScale Biomaterials, Waterloo, ON, Canada). All samples were attached

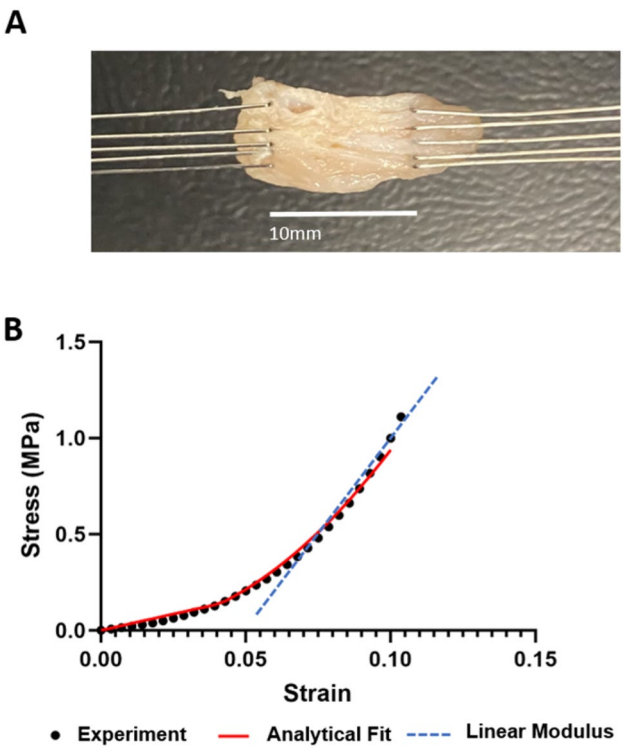

Fig. 2 **A** Example of experimental set up to obtain tissue mechanical properties using CellScale BioRakes. **B** Representative example of the obtained experimental stress-strain curves of the supraspinatus tendon, showing the analytical fit, and obtained linear modulus

to the testing system using CellScale BioRakes, designed for soft tissue testing to reduce clamp strain-induced errors (Fig. 2A). Samples were ramped to 10% strain at a strain rate of 0.1%/s (0.1 mm/s) [31] and underwent three

preconditioning cycles to remove excess slack in the system and ensure consistent data collection, followed by data acquisition on the subsequent cycle. Tendons may be elastically stretched up to 14% strain [42], thus each region was only tested to 10% strain to ensure the specimens did not undergo permanent deformation for subsequent histological evaluation of collagen fibers. During testing, specimen hydration was maintained with 0.9% saline. Four measurements on each side of the specimens were taken with a digital caliper to measure sample thickness to calculate the cross-sectional area, which was then used to calculate stress. A custom in-house MATLAB (MATLAB 2023, MathWorks, Natick, MA, USA) code was employed to estimate tissue Cauchy stress and Green strain (Fig. 2B). The linear modulus was calculated from each stress–strain curve via linear regression,[43,44] to evaluate the differences in the mechanical properties for each region (Fig. 2B).

Histological Evaluation of Collagen Fibers

Collagen fibers are the main structural unit in tendon, playing an important role in tendon mechanical behavior. After mechanical testing, we carefully removed the tissue from the testing apparatus. For histological preparations of tendon samples, the tissue was fixed with 10% neutral buffer formalin and embedded in paraffin for histological sectioning at BIDMC Histology Core. The samples were cut along the length of the tendon every 250 µm, resulting in 3 samples per tendon region, and stained using Masson's trichrome staining. Next, we acquired high-resolution images of each stain under a 10 × brightfield microscope (Olympus VS 120, Evident Olympus Scientific Solutions, Waltham, MA, USA). Fiber orientation distribution for all sections was quantified via ImageJ's OrientationJ plugin [45]. To approximate the fiber distribution as a probability density function, we used non-linear least squares regression to fit the transversely isotropic and π periodic von Mises distribution (Eq. 1) [46], where θ is the fiber orientation and b is the concentration parameter.

$$p(\theta) = 4\sqrt{\frac{b}{2\pi}}\frac{\exp[b(\cos(2\theta)+1)]}{erfi\left(\sqrt{2b}\right)} \tag{1}$$

Material Fitting

Characterizing the material response accurately is imperative to define materials to be used as inputs for FE modeling of soft tissue. Stress–strain curves from each region were fit to the Holzapfel-Gasser-Ogden (HGO) hyper-elastic fiber-reinforced model (Fig. 2B), commonly used to model soft tissue (Eq. 2) [46]:

$$U = C_{10}\left(\overline{I}_1 - 3\right) + \frac{k_1}{2k_2}\sum_{a=1}^{N}\left\{\exp\left[k_2\left\langle \chi\left(\overline{I}_1 - 3\right) + (1-3\chi)\left(\overline{I}_4 - 1\right)\right\rangle^2\right] - 1\right\} \tag{2}$$

where C10 is the isotropic modulus of the ground substance; k1 is the effective (linear) modulus of the collagen fibers; k2 is the rate of exponential stiffening of the fibers when stretched along their end-to-end axes (M–L direction); and κ is a fiber ''dispersion parameter'' that measures how aligned, or not, the collagen fibers are. $\overline{I}_1$ and $\overline{I}_4$ represent the 1st and 4th invariants of the Cauchy stress tensor, respectively. Previous studies have worked under the assumption that the fibers were aligned along the length of the tendon in a transversely isotropic manner [32,33,39]. However, this may not always be the case as the supraspinatus has variation in collagen fiber orientation [36–38]. Thus, κ was calculated from histological data by mapping the probability density parameter 'b' to κ as described by Holzapfel [46] and input for each specimen when performing curve fitting. Minimizing the root mean square error (RMSE) between the estimated curve and the raw data using MATLAB's 'fminsearch' optimization function ensured that regional material response was adequately captured [47].

Finite Element Model Formulation

To accurately capture the supraspinatus (SSP) and infraspinatus (ISP) geometry, a previously validated FE model of the supraspinatus and the infraspinatus was used [39]. This model was able to predict the increasing supraspinatus tendon strain with increasing loads (5, 10, 15, 20, and 25 lbs) on the infraspinatus tendon, showing the important interaction between these two tendons of the RC. Furthermore, this model was validated within 3% absolute strain by capturing the surface strain on both the articular and bursal surface of a cadaveric specimen under similar loading conditions. This identified the validity of model geometry when complex loading conditions are applied, rather than simply loading the supraspinatus tendon only, allowing for a more comprehensive evaluation of the mechanical environment of the supraspinatus tendon [39].

The model was imported into 3-matic (Mimics Materialize and 3-Matic, Leuven, Belgium) to create various mesh sizes for a mesh sensitivity analysis. This ensured all results were independent of mesh size. Mesh sizes were created by decreasing the edge length of the elements, until less than 0.2% strain difference was found between meshes. This resulted in an average edge length of 0.8 mm, consisting of 225,356 elements and 36,827 nodes. To create the sub-regions, a custom MATLAB code was used to split the

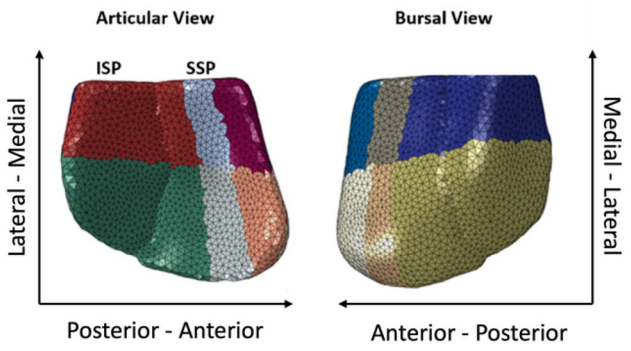

Fig. 3 Finite element model showing the 12 regions tested and applied to the model

supraspinatus in the center of the posterior third of the tendon to create models representing posterior-sided tears expanding anteriorly. To create models representing tears originating in the middle region of the tendon, crescent-shaped cuts were created on the supraspinatus from the center of the middle region and expanded equally on both the anterior and posterior sides. Tear sizes were determined as a percentage based on the width of the supraspinatus at the lateral edge. All tears were created on the lateralmost edge to mimic RC tears at the osteotendinous insertion (Fig. 4). This resulted in two small (< 1 cm or equivalent to 20-30% of the tendon width) and two medium (1-3 cm or equivalent to 40-50% of the tendon width) supraspinatus tears.

Finite Element Simulations

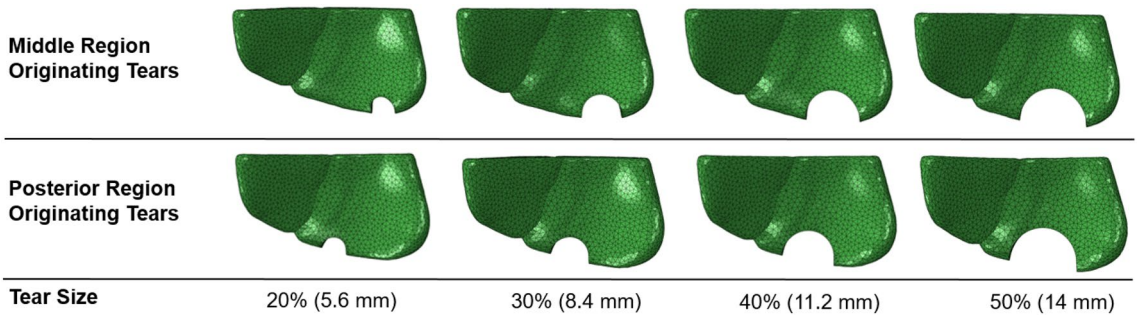

Fig. 4 Finite element models for middle and posterior crescent-shaped tears ranging from 20% (5.6 mm) to 50% (14 mm) of the tendon width.

nodes and the elements into 12 equal regions of the same volume (Fig. 3), matching the experimentally tested regions. To assess how specimen-specific material properties from different specimens alter the FE predicted tendon strain, six FE models were created. Material properties were assigned to the sub-regions of the supraspinatus mesh that matched those tested during uniaxial tensile tests based on the HGO material constants obtained during the material fitting phase for each of the 6 specimens tested. The mechanical properties of the infraspinatus were not tested, so it was assigned the same material properties as the posterior regions of the supraspinatus [32,33].

Finite Element Tear Model Creation

Clinically, crescent-shaped tears are the most commonly seen RC tear types [26], often defined by size, with small, medium, and large tears being < 1 cm, 1-3 cm, and 3-5 cm, respectively [48]. Previous studies measuring the size of RC tears have found that the A-P and M–L tear lengths are roughly the same for small- and medium-sized tears [27,49–51]. Furthermore, recent studies have suggested that RC tears originate more posterior than previously thought [27,28]. Crescent-shaped cuts were made on the

All FE simulations were conducted in ABAQUS (2023, Dassault Systèmes, Vélizy-Villacoublay, France) using a standard static simulation over a maximum of 100 steps to ensure convergence of the simulation. The supraspinatus tendon was constrained in all directions from the lateral edge to 1.7 mm above the edge to mimic the supraspinatus tendon insertion [52] and followed along the infraspinatus. The forces were applied to the medial edge of the supraspinatus and infraspinatus for all models [39]. For model validation loads, the supraspinatus was loaded at 135 N. The supraspinatus tendon was first loaded for the RC tears models until a failure strain of 26.1% [53] occurred at the tear tips. For daily living and physical therapy exercises, the supraspinatus and infraspinatus loads were calculated based on the peak in vivo forces experienced by the tendons and scaled by tendon-specific maximum voluntary isometric contractile values (MVIC) to determine the activity-specific loading conditions (Eq 3.)

$$Force = Peak\,Force \times \%MVIC \tag{3}$$

Based on muscle architecture, reported peak in vivo force for the supraspinatus and infraspinatus is 370 N and 773 N, respectively [54]. The reported MVIC of the

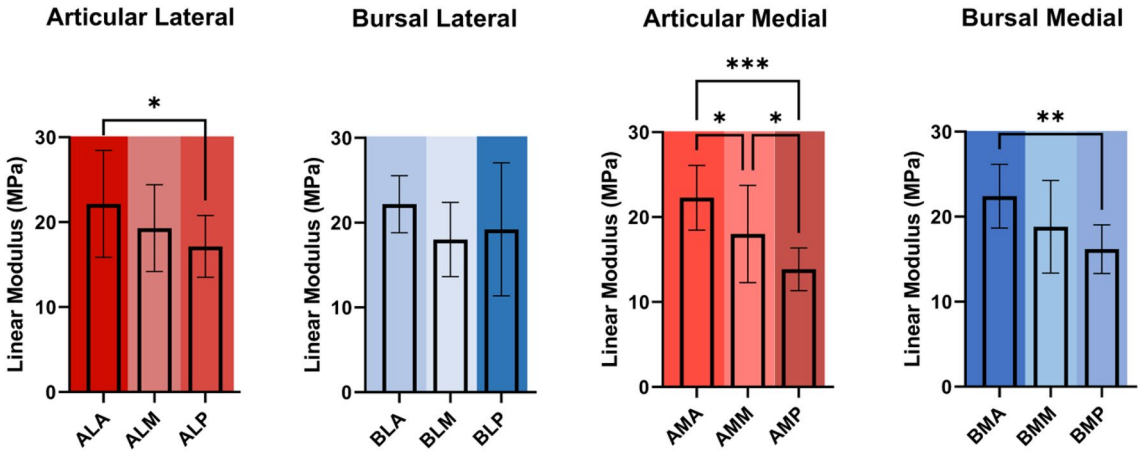

Fig. 5 Measured tendon modulus for each region tested. Individual graphs show the variations from anterior—posterior modulus, as there were no differences observed between medial—lateral and articular—bursal planes. Marked colors correspond to the same regions as Fig. 1. '*' represents $p < 0.05$, '**' represents $p < 0.01$, '***' represents $p < 0.001$.

supraspinatus and infraspinatus muscles for the following daily activities [55] and physical therapy exercises [56] were: drinking (supraspinatus = 21%, infraspinatus 18.3%), brushing teeth (supraspinatus = 12%, infraspinatus = 18%), external rotation at 90° abduction (supraspinatus = 57%, infraspinatus 50%), and prone abduction (supraspinatus = 82%, infraspinatus = 39%). This resulted in the following loads being applied to each model: drinking (supraspinatus = 78 N, infraspinatus = 141 N), brushing teeth (supraspinatus 45 N, infraspinatus 156 N), external rotation at 90° abduction (supraspinatus = 211 N, infraspinatus 387 N), and prone abduction (supraspinatus = 303 N, infraspinatus 301 N). While these estimates are muscle forces, it was assumed that all force generated from the muscle was transferred to the tendon.

The output for all simulations resulted in nodal logarithmic strains, which were converted to maximum principal Lagrangian strain for each node of the supraspinatus tendon. For model validation, the strain was averaged in the bottom third of the tendon above the insertion, matching the location of the cadaveric experiment [41]. The strain was averaged for all nodes within 2 mm adjacent to the tear to evaluate the strain for the models with tears.

Statistical Analysis

The Shapiro–Wilk test was used to assess the normality of the data. Normal distribution was reported for the mechanical properties and FE data. Mechanical properties were analyzed using a one-way repeated measure ANOVA. A Fisher's LSD *post hoc* test was used for comparisons between regions. FE Data were analyzed using two-way repeated measure ANOVA, where "Tear Size" and "Region" (posterior tip and anterior tip) were treated as within-subject factors. The Tukey *post hoc* test was used for multiple comparisons of simple effects of the region on percent strain for each tear size. Statistical analysis was performed using GraphPad Prism unless otherwise noted (version 9.3.1 for Windows, GraphPad Software, San Diego, CA, USA). Two-tailed p-values less than 0.05 were considered significant.

Results

Heterogeneity of Supraspinatus Mechanical Properties

Analysis of the 12 regions of the supraspinatus tendon indicated that the anterior region is generally the stiffest, with the linear modulus decreasing posteriorly (Fig. 5). This trend was found in the articular lateral region (ALA > ALP, $p = 0.0442$), articular medial region (AMA > AMP, $p = 0.0005$; AMA > AMM, $p = 0.029$; AMM > AMP, $p = 0.033$), and the bursal medial region (BMA > BMP $p = 0.004$). However, in the bursal lateral region, no significant differences were found in linear modulus between regions. No significant differences were found between the articular and bursal regions or the medial and lateral regions.

Finite Element Model Validation

The ability to accurately predict tissue deformation is an important aspect of FE models for clinical applicability [40]. Such validation requires comparing cadaveric data to the FE model to determine the model's predictive capability [57]. Our models had an average maximum principal strain of $6.87 \pm 0.92\%$ (range 5.24–7.73%) and $10.21 \pm 1.07\%$ (range 8.34–11.23%) for the articular and bursal sides, respectively.

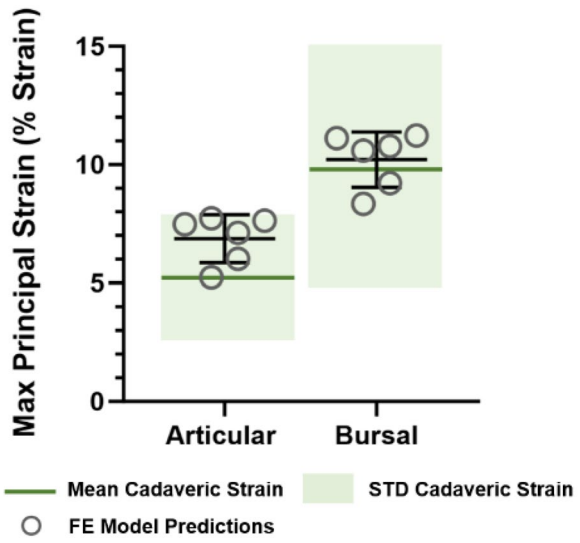

Fig. 6 Finite element model predictions compared to the mean and standard deviation from cadaveric experiments in literature.

validated and could be used to study the effects of RC tears on the strain experienced by the supraspinatus tendon.

Failure Loads for Varying Tear Size and Location

To assess the differences based on tear location, failure loads were determined for tears in the middle and posterior regions (Fig. 7A), where the average strain at the posterior or anterior tip reached the failure strain of 26.1% (Fig. 7B). Generally, failure strain decreased as tear size increased. However, for all tear sizes, there were no significant differences in failure load between tears in the middle and posterior regions (Table 1). However, what was revealed was that there were substantial differences (max% difference: 48%) from specimen to specimen for the failure load, suggesting that patient-specific material properties play an important role in RC tears (Table 1). Middle tears had a larger percent difference between specimens than posterior-sided tears for all cases and generally decreased with increasing tear size.

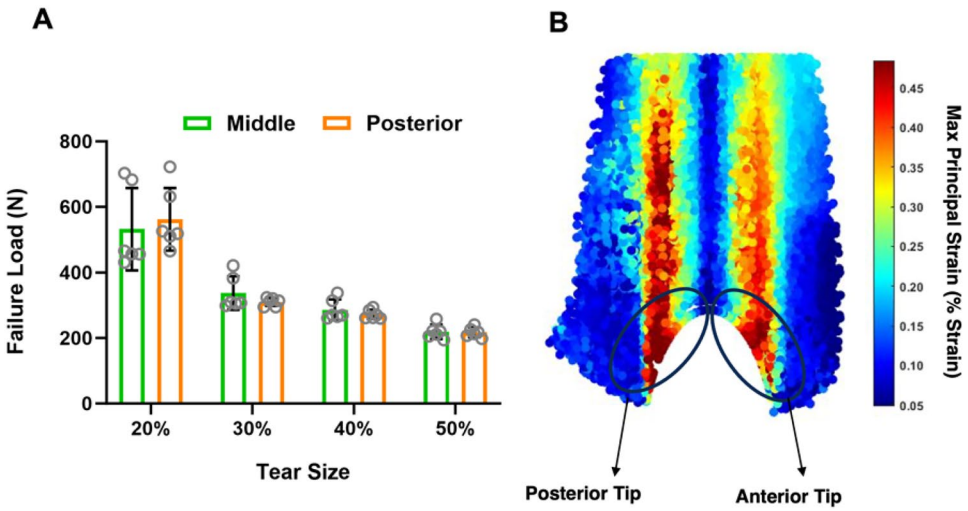

Fig. 7 **A** Failure loads for middle and posteriorly located tears with increasing tear size. **B** Representative finite element results with regions averaged to assess the tear tips

The FE model was considered validated when the articular- and bursal-sided strain at the bottom third, just above the insertion, was within the range of previously reported cadaveric data ($5.4 \pm 2.5\%$ and $10.6 \pm 5.6\%$ for the articular and bursal sides, respectively) [41], and was within 3% of the absolute strain of the mean cadaveric strain [39,58]. All models fell within the range of reported strain for the supraspinatus tendon subjected to 135 N load (Fig. 6) and were able to predict tendon strain within an absolute value of 3% strain on both the articular (range of absolute difference: 0.16–2.33% strain) and bursal (range of absolute difference: 0.002–2.25% strain) surfaces. Since all models were within the range of previously reported strains and were within the threshold of 3% absolute strain, the models were considered

Supraspinatus Tendon Strain for Daily Living Activities

During loading conditions that mimic the forces experienced on the supraspinatus and infraspinatus during activities of daily living, tendon strain at both the anterior and posterior tear tips increased with tear size for the middle tears (Fig. 8). However, for the posterior-sided tears, the strain at the anterior tear tip slightly decreased while the strain at the posterior tear tip increased (Fig. 8). For tears located in the middle region of the supraspinatus tendon, there was significantly more strain posteriorly for small tears during both drinking (20%, $p < 0.0001$; 30%, $p < 0.0001$) and brushing teeth (20%, $p = 0.002$; 30%,

Table 1 Failure loads and maximum percent difference between models with middle and posterior tears

Tear size	Posterior tears Failure load (N)	Posterior tears Maximum % difference	Middle tears Failure load (N)	Middle tears Maximum % difference
20%	562.16 ± 95.63 N	43%	532.33 ± 125.11	48%
30%	310.61 ± 12.60 N	9%	337.60 ± 51.52 N	34%
40%	272.39 ± 14.07 N	12%	286.54 ± 31.95 N	25%
50%	218.81 ± 21.96 N	20%	217.38 ± 15.04 N	10%

$p = 0.005$). For posterior-sided tears, there was no difference in tear tip strain at the anterior and posterior tear tips, apart from the 20% tears for both drinking ($p = 0.012$) and brushing teeth ($p = 0.011$).

Supraspinatus Tendon Strain for Physical Therapy Activities

During loading conditions that mimic the forces experienced on the supraspinatus and infraspinatus tendons during physical therapy exercises, tendon strain at both the anterior and posterior tear tips increased with tear size for the middle and posterior tears (Fig. 9). For tears located in the middle region of the supraspinatus tendon, the strain on the posterior tear tip was larger than the anterior tear tip for small tears during both prone abduction (20%, $p < 0.0002$; 30%, $p < 0.0023$) and external rotation at 90° abduction (20%, $p = 0.0002$; 30%, $p = 0.001$). For posterior-sided tears, there was no difference in tear tip strain, apart from the 40% tears for external rotation at 90° abduction ($p = 0.0324$). For medium-sized full-thickness tears (40% and 50%), the maximum principal strain at tear tips exceeded the failure criteria of 26.1% strain for both the middle and posteriorly located tears for prone abduction. However, one model with a middle tear was below this threshold. On the other hand, three models with 30% posterior tears were above the failure threshold of 26.1%. Generally, medium-sized tears subjected to forces experienced during external rotation at 90° abduction did not reach the failure criteria. However, one model with a middle tear and two with posterior tears exceeded the failure strain at the tear tips.

Discussion

This study establishes the validation of a three-dimensional supraspinatus-infraspinatus FE model with heterogeneous material properties, which was then used to study tissue deformation as tear location and tear size changes during activities of daily living and common physiotherapy exercises. Validation demonstrated that all FE models could accurately predict strain within 3% absolute strain of the reported strain from cadaveric experiments. The primary finding of our study was the development of an FE model to assess changes to the mechanical environment from varying material properties, tear location, and tear size. Furthermore, small- and medium-sized full-thickness tears are unlikely to experience rapid tear progression from the tested activities of daily living. However, medium-sized full-thickness tears, regardless of tear location and material properties, are at a higher risk for tear progression during physiotherapy exercises as they reach failure strain for loads corresponding to prone abduction.

The propensity for RC tears to progress is poorly understood, making the appropriate treatment methods difficult to identify. The structural and mechanical heterogeneity of the supraspinatus tendon is important to understand to fully capture the mechanical environment of the supraspinatus tendon and how and why tears may be at risk of progressing [29,41,59]. More importantly, how tears alter the mechanical environment and change tissue strain is crucial in identifying the appropriate treatment methods. Previous FE studies examining how tears affect tissue strain have found that increases in tear size significantly alter the mechanical environment of the supraspinatus tendon and increase the maximum principal strain surrounding the tear tips [32–34,60]. While these studies provide valuable insight into the alterations of the mechanical environment of the supraspinatus, there are still limitations hindering the clinical applicability of these models. By using collagen fiber-informed material properties to capture the spatial heterogeneity of the non-linear mechanical properties of the tendon, clinically relevant tear shapes, and loading conditions experienced in vivo, we have attempted to better understand how patient-specific material properties, tear location, and tear size affect tissue strain during activities of daily living and physiotherapy exercises to help guide clinical management.

The development of our FE model and its demonstrated validity in simulating tendon tear progression holds significant implications for orthopedic surgeons and the clinical management of symptomatic patients with supraspinatus tears. In clinical practice, managing such tears remains a challenging dilemma, with ongoing debate regarding the optimal approach. Traditionally, a conservative treatment approach is often the initial choice, with surgical intervention

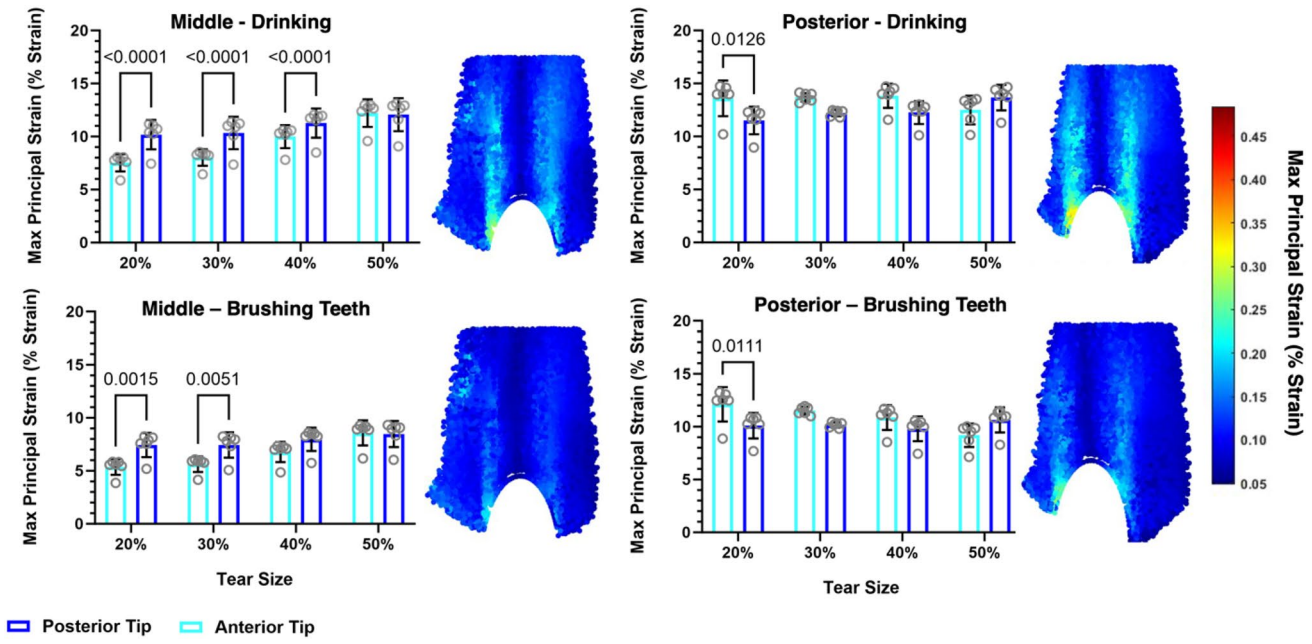

Fig. 8 Results of daily living activities (Drinking and Brushing teeth) with increasing tear size for middle and posterior sided tears. Finite element heat maps represent the supraspinatus tendon strain with 50% tears

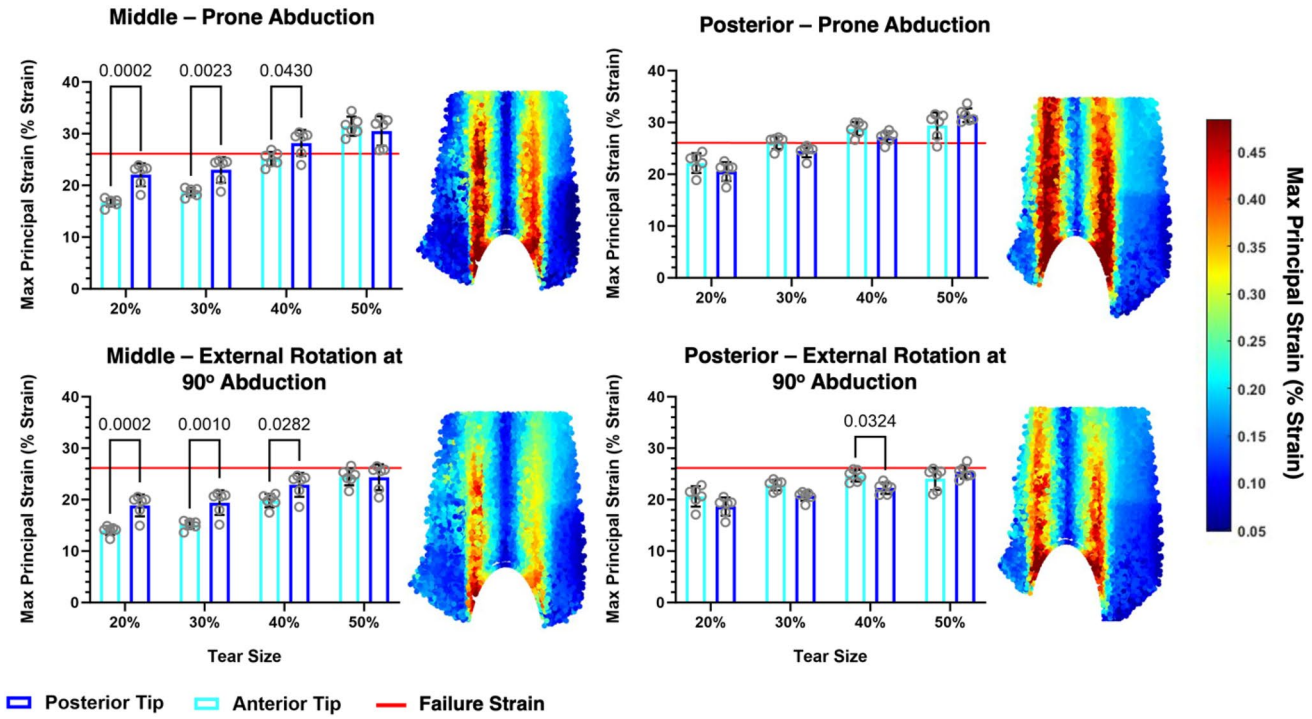

Fig. 9 Results of daily living activities (Drinking and Brushing teeth) with increasing tear size for middle and posterior sided tears. Finite element heat maps represent the supraspinatus tendon strain with 50% tears

reserved for patients who do not respond favorably [61]. However, this cautious approach can sometimes result in delayed surgical intervention, leading to larger and more complex tears, yielding less favorable clinical outcomes [62]. A prospective randomized control trial by Ranebo et al. showed that 29% of patients that underwent physiotherapy

without tendon repair had tear progression > 5 mm after just one year of follow-up [63]. The prescribed physiotherapy exercises included active unloaded elevation, external, and internal rotation, and isometric strengthening exercises [64,65], which are similar to the actives studied here. Given the worse surgical outcomes with increased RC tear size, it is important to understand which patients will be at risk of progression from physiotherapy.

Our study contributes to this critical area of clinical decision-making by shedding light on the likelihood of tear progression in various supraspinatus tear sizes and locations. This insight can enable more informed and timely clinical decisions, potentially preventing the advancement of tears to more challenging stages. Treatment with physiotherapy for small- and medium-sized RC tears was reported to be insufficient for 27% of patients over a 10-year follow-up [6]. Current guidelines developed by the American Academy of Orthopedic Surgeons suggest that physiotherapy is an appropriate management method for small- to medium-sized RC tears. However, it should be noted that tear size, muscle atrophy, and fatty infiltration may progress over 5 to 10 years [66]. Our FE study supports these recommendations, showing that small tears are unlikely to reach failure strain during common physiotherapy exercises where the supraspinatus is most active. However, for posterior-sided tears, three models with 30% thickness tears (small tear) reached failure strain during loading conditions that mimic prone abduction. This suggests that tendon-specific material properties also play an important role in assessing RC health and the risk for tear progression. Furthermore, no unanimous failure was reported for medium-sized tears. One model with a middle tear and two models with posterior tears exceeded the failure strain at the tear tips for external rotation at 90° abduction. On the other hand, one model did not fail during prone abduction. This suggests that tendon-specific material properties play an important role in evaluating the likelihood of tear progression. Overall, more targeted patient management plans are needed based on tear location, tear size, and tendon material properties to avoid strenuous exercises that could cause tear propagation. Our findings highlight that exercises involving prone abduction could potentially put patients at risk for tear progression due to the increased tissue strain. However, clinical studies are needed to confirm these findings. Ultimately, this would lead to more successful outcomes in physiotherapy and reduce the need for secondary tendon repair, with the added risk of worse outcomes due to tear progression following physiotherapy.

Understanding how rotator cuff tears alter the mechanical environment of the supraspinatus is crucial for comprehending the natural progression of these lesions. Moreover, how these tears progress is based on the increased strain surrounding the tear site. While the exact location of tear initiation remains uncertain, we do know that tears originate more posteriorly than originally thought [27,28]. Based on our results, tears in the middle region are more likely to progress posteriorly, as there was significantly more strain at the posterior tip compared to the anterior tip. This could be because the anterior supraspinatus is significantly stiffer and mechanically stronger than the posterior supraspinatus.

Interestingly, we saw a slight decrease in the anterior tear tip strain for daily living activities as tear size increased for posteriorly originating tears. One possible explanation for this could be that as the tear increased, the load was distributed anteriorly into a mechanically stiffer tendon region. However, we did not see differences in the tear tip strain for posterior tears, suggesting that tears originating posteriorly may further progress into the supraspinatus or the infraspinatus. This is important because progression into massive tears (i.e., tears involving two tendons) has significantly worse clinical outcomes [67]. Furthermore, it has been reported that large tears account for 40% of all RC tears [68]. Thus, understanding patient-specific tendon mechanical properties, tear size, and location is imperative to better treatment of RC tears to reduce the risk of tear progression, ultimately leading to worse clinical outcomes.

Although it is important to interpret these results, time is a pivotal variable in the progression of tendon tears. While our study demonstrates that typical daily activity forces do not immediately lead to tear progression, it's essential to acknowledge the longitudinal aspect of tear development. The study by Torchia et al. [69], with a median follow-up duration of 7.1 years, presents compelling evidence of tear enlargement in 60% of partial-thickness tears over time. The stability observed during daily activities, as demonstrated in our study, may not necessarily translate into stability over extended periods. Importantly, collagen breakdown due to repetitive fatigue damage over time can lead to an increased risk for structural failure [70]. This could be the mechanism that causes failure over long periods, even under low-loading conditions. Moreover, this could be a potential reason why RC tears progress slowly over time during activities of daily living and see more progression during physiotherapy, as the tendon is under significantly higher strain.

While this model only examined a few activities of daily living and physiotherapy exercises, it provides valuable insight into the changes in tissue deformation. Furthermore, this model may measure different loads (i.e., other activities of daily living or physiotherapy exercises) and tear shapes, such as U-shaped or L-shaped tears, which comprise 25% and 21% of RC tears seen clinically, respectively [26]. This model provides a better understanding of the strain on the supraspinatus, which may cause tear progression. Such insight allows for a more tailored approach to clinical management, such as physiotherapy recommendations or activities to avoid that could result in tear progression. While this must be clinically evaluated, it is a step forward

in understanding tear progression and how it can modify patient care.

Limitations

Limitations of this study include those common with all cadaveric studies [71], including using dead tissue to simulate in vivo tendon strain, not accounting for the effects of tissue degeneration, and not including the teres minor and subscapularis. However, the model was able to capture and predict tissue strains that matched cadaveric data successfully. Therefore, the strains associated with the models with tears may be more accurate than previous studies and provide insight into loading conditions specific to activities of daily living and physiotherapy. However, it should be mentioned the muscle forces used represent generalized force profiles taken from healthy, age-matched individuals with RC tears [54], which does not account for changes in muscle activity for patients with RC tears. This may alter the results as individual patients may have experienced different force profiles, but since there is no available data on muscle activation changes based on tear size, this is the best representation of physiologically relevant forces. To fully capture the effects of RC tears in alterations of the mechanical environment of the supraspinatus tendon, a more comprehensive evaluation of the mechanical properties as tendons degenerate is needed. However, only one study has evaluated how degenerative changes, determined by a semiquantitative histological assessment, affect the ultimate tensile load of the supraspinatus at the osteotendinous insertion [72]. Therefore, a method to better quantify tendon degeneration is needed to detect changes in the tendon non-invasively. This study aimed to investigate the changes in small- and medium-sized RC tears isolated to the supraspinatus tendons. The exclusion of the teres minor and subscapularis was due to the fact that they have minimal loading effect on the supraspinatus tendon [20].

Conclusion

We developed a validated three-dimensional supraspinatus-infraspinatus FE model with heterogeneous material properties. The findings from this study provide a better understanding of the mechanical environment of the supraspinatus tendon with small- and medium-sized supraspinatus tears during activities of daily living and physiotherapy. Clinical imaging modalities (MRI and US) are typically used to assess the size of RC tears, where tear size could potentially guide physical therapy interventions. Small tears seem unlikely to progress based on the regional strain response; however, medium-sized tears are at higher risk during more strenuous physiotherapy exercises. Moreover, the difference in material properties from tendon to tendon is also important to better understand the risk for tear progression. Therefore, patient-specific management plans based on tear size, location, and tendon material properties could improve clinical outcomes.

Funding The Joe Fallon Research Fund and the Dr. Louis Meeks BIDMC Sports Medicine Trainee Research Fund at BIDMC Orthopaedic Surgery Department funded this study.

Declarations

Conflict of interest The authors have no relevant financial or non-financial interests to disclose.

References

1. Yamaguchi, K., K. Ditsios, W. D. Middleton, et al. The demographic and morphological features of rotator cuff disease. A comparison of asymptomatic and symptomatic shoulders. *J. Bone Jt. Surg. Am.* 88(8):1699–1704, 2006.
2. Mall, N. A., H. M. Kim, J. D. Keener, et al. Symptomatic progression of asymptomatic rotator cuff tears: a prospective study of clinical and sonographic variables. *J. Bone Jt. Surg. Am.* 92(16):2623–2633, 2010.
3. Moosmayer, S., R. Tariq, M. Stiris, and H. J. Smith. The natural history of asymptomatic rotator cuff tears: a three-year follow-up of fifty cases. *J. Bone Jt. Surg Am.* 95(14):1249–1255, 2013.
4. Safran, O., J. Schroeder, R. Bloom, Y. Weil, and C. Milgrom. Natural history of nonoperatively treated symptomatic rotator cuff tears in patients 60 years old or younger. *Am. J. Sports Med.* 39(4):710–714, 2011.
5. Schmidt, C. C., C. D. Jarrett, and B. T. Brown. Management of rotator cuff tears. *J. Hand Surg. Am.* 40(2):399–408, 2015.
6. Moosmayer, S., G. Lund, U. S. Seljom, et al. At a 10-year follow-up, tendon repair is superior to physiotherapy in the treatment of small and medium-sized rotator cuff tears. *J. Bone Jt. Surg. Am.* 101(12):1050–1060, 2019.
7. Edwards, P., J. Ebert, B. Joss, et al. EXERCISE REHABILITATION IN THE NON-OPERATIVE MANAGEMENT OF ROTATOR CUFF TEARS: A REVIEW OF THE LITERATURE. *Int. J. Sports Phys. Ther.* 11(2):279–301, 2016.
8. Bassett, R. W., A. O. Browne, B. F. Morrey, and K. N. An. Glenohumeral muscle force and moment mechanics in a position of shoulder instability. *J. Biomech.* 23(5):405–415, 1990.
9. Bigliani, L. U., R. Kelkar, E. L. Flatow, R. G. Pollock, and V. C. Mow. Glenohumeral stability. Biomechanical properties of passive and active stabilizers. *Clin. Orthop. Relat. Res.* 330:13–30, 1996.
10. Blasier, R. B., L. J. Soslowsky, D. M. Malicky, and M. L. Palmer. Posterior glenohumeral subluxation: active and passive stabilization in a biomechanical model. *J. Bone Jt. Surg. Am.* 79(3):433–440, 1997.
11. McMahon, P. J., R. E. Debski, W. O. Thompson, et al. Shoulder muscle forces and tendon excursions during glenohumeral abduction in the scapular plane. *J. Shoulder Elbow Surg.* 4(3):199–208, 1995.
12. Soslowsky, L. J., D. M. Malicky, and R. B. Blasier. Active and passive factors in inferior glenohumeral stabilization: a biomechanical model. *J. Shoulder Elbow Surg.* 6(4):371–379, 1997.

13. Gomoll, A. H., J. N. Katz, J. J. Warner, and P. J. Millett. Rotator cuff disorders: recognition and management among patients with shoulder pain. *Arthritis Rheum.* 50(12):3751–3761, 2004.
14. Matava, M. J., D. B. Purcell, and J. R. Rudzki. Partial-thickness rotator cuff tears. *Am. J. Sports Med.* 33(9):1405–1417, 2005.
15. Terry, G. C., and T. M. Chopp. Functional anatomy of the shoulder. *J. Athl. Train.* 35(3):248–255, 2000.
16. Woodward, T. W., and T. M. Best. The painful shoulder: part I. Clinical evaluation. *Am. Fam. Phys.* 61(10):3079–3088, 2000.
17. Yamanaka, K. Pathological study of the supraspinatus tendon. *Nihon Seikeigeka Gakkai Zasshi.* 62(12):1121–1138, 1988.
18. Andarawis-Puri, N., A. F. Kuntz, S. Y. Kim, and L. J. Soslowsky. Effect of anterior supraspinatus tendon partial-thickness tears on infraspinatus tendon strain through a range of joint rotation angles. *J. Shoulder Elbow Surg.* 19(4):617–623, 2010.
19. Andarawis-Puri, N., A. F. Kuntz, M. L. Ramsey, and L. J. Soslowsky. Effect of glenohumeral abduction angle on the mechanical interaction between the supraspinatus and infraspinatus tendons for the intact, partial-thickness torn, and repaired supraspinatus tendon conditions. *J. Orthop. Res.* 28(7):846–851, 2010.
20. Andarawis-Puri, N., E. T. Ricchetti, and L. J. Soslowsky. Interaction between the supraspinatus and infraspinatus tendons: effect of anterior supraspinatus tendon full-thickness tears on infraspinatus tendon strain. *Am. J. Sports Med.* 37(9):1831–1839, 2009.
21. Namdari, S., R. P. Donegan, N. Dahiya, et al. Characteristics of small to medium-sized rotator cuff tears with and without disruption of the anterior supraspinatus tendon. *J. Shoulder Elbow Surg.* 23(1):20–27, 2014.
22. Codman, E. A., and I. B. Akerson. THE PATHOLOGY ASSOCIATED WITH RUPTURE OF THE SUPRASPINATUS TENDON. *Ann. Surg.* 93(1):348–359, 1931.
23. Hijioka, A., K. Suzuki, T. Nakamura, and T. Hojo. Degenerative change and rotator cuff tears. An anatomical study in 160 shoulders of 80 cadavers. *Arch. Orthop. Trauma Surg.* 112(2):61–64, 1993.
24. Keyes, E. L. Observations on rupture of the supraspinatus tendon: based upon a study of seventy-three cadavers. *Ann. Surg.* 97(6):849–856, 1933.
25. Lehman, C., F. Cuomo, F. J. Kummer, and J. D. Zuckerman. The incidence of full thickness rotator cuff tears in a large cadaveric population. *Bull. Hosp. Jt. Dis.* 54(1):30–31, 1995.
26. Watson, S., B. Allen, C. Robbins, et al. Does the rotator cuff tear pattern influence clinical outcomes after surgical repair? *Orthop. J. Sports Med.* 6(3):2325967118763107, 2018.
27. Kim, H. M., N. Dahiya, S. A. Teefey, et al. Location and initiation of degenerative rotator cuff tears: an analysis of three hundred and sixty shoulders. *J. Bone Jt. Surg. Am.* 92(5):1088–1096, 2010.
28. Jeong, J. Y., S. K. Min, K. M. Park, et al. Location of rotator cuff tear initiation: a magnetic resonance imaging study of 191 shoulders. *Am. J. Sports Med.* 46(3):649–655, 2018.
29. Itoi, E., L. J. Berglund, J. J. Grabowski, et al. Tensile properties of the supraspinatus tendon. *J. Orthop. Res.* 13(4):578–584, 1995.
30. Lake, S. P., K. S. Miller, D. M. Elliott, and L. J. Soslowsky. Tensile properties and fiber alignment of human supraspinatus tendon in the transverse direction demonstrate inhomogeneity, nonlinearity, and regional isotropy. *J. Biomech.* 43(4):727–732, 2010.
31. Lake, S. P., K. S. Miller, D. M. Elliott, and L. J. Soslowsky. Effect of fiber distribution and realignment on the non-linear and inhomogeneous mechanical properties of human supraspinatus tendon under longitudinal tensile loading. *J. Orthop. Res.* 27(12):1596–1602, 2009.
32. Miller, R. M., J. Thunes, S. Maiti, V. Musahl, and R. E. Debski. Effects of tendon degeneration on predictions of supraspinatus tear propagation. *Ann. Biomed. Eng.* 47(1):154–161, 2019.
33. Miller, R. M., J. Thunes, V. Musahl, S. Maiti, and R. E. Debski. Effects of tear size and location on predictions of supraspinatus tear propagation. *J. Biomech.* 68:51–57, 2018.
34. Quental, C., J. Folgado, J. Monteiro, and M. Sarmento. Full-thickness tears of the supraspinatus tendon: a three-dimensional finite element analysis. *J. Biomech.* 49(16):3962–3970, 2016.
35. Quental, C., J. Reis, J. Folgado, J. Monteiro, and M. Sarmento. Comparison of 3 supraspinatus tendon repair techniques—a 3D computational finite element analysis. *Comput. Methods Biomech. Biomed. Eng.* 23(16):1387–1394, 2020.
36. Clark, J. M., and D. T. Harryman 2nd. Tendons, ligaments, and capsule of the rotator cuff. Gross and microscopic anatomy. *J. Bone Jt. Surg. Am.* 74(5):713–725, 1992.
37. Gohlke, F., B. Essigkrug, and F. Schmitz. The pattern of the collagen fiber bundles of the capsule of the glenohumeral joint. *J. Shoulder Elbow Surg.* 3(3):111–128, 1994.
38. Nakajima, T., N. Rokuuma, K. Hamada, T. Tomatsu, and H. Fukuda. Histologic and biomechanical characteristics of the supraspinatus tendon: Reference to rotator cuff tearing. *J. Shoulder Elbow Surg.* 3(2):79–87, 1994.
39. Williamson, P., M. Garcia, K. Momenzadeh, et al. A validated three-dimensional, heterogenous finite element model of the rotator cuff and the effects of collagen orientation. *Ann. Biomed. Eng.* 51(5):1002–1013, 2023.
40. Viceconti, M., S. Olsen, L. P. Nolte, and K. Burton. Extracting clinically relevant data from finite element simulations. *Clin. Biomech. (Bristol, Avon).* 20(5):451–454, 2005.
41. Huang, C. Y., V. M. Wang, R. J. Pawluk, et al. Inhomogeneous mechanical behavior of the human supraspinatus tendon under uniaxial loading. *J. Orthop. Res.* 23(4):924–930, 2005.
42. Wang, J. H., M. I. Iosifidis, and F. H. Fu. Biomechanical basis for tendinopathy. *Clin. Orthop. Relat. Res.* 443:320–332, 2006.
43. Lake, S. P., J. G. Snedeker, V. M. Wang, et al. Guidelines for ex vivo mechanical testing of tendon. *J. Orthop. Res.* 41(10):2105–2113, 2023.
44. Nesbitt, D. Q., M. L. Nelson, K. S. Shannon, and T. J. Lujan. Dots-on-plots: a web application to analyze stress-strain curves from tensile tests of soft tissue. *J. Biomech. Eng.* 145(2):024504, 2023.
45. Rezakhaniha, R., A. Agianniotis, J. T. Schrauwen, et al. Experimental investigation of collagen waviness and orientation in the arterial adventitia using confocal laser scanning microscopy. *Biomech. Model Mechanobiol.* 11(3–4):461–473, 2012.
46. Gasser, T. C., R. W. Ogden, and G. A. Holzapfel. Hyperelastic modelling of arterial layers with distributed collagen fibre orientations. *J. R. Soc. Interface*. 3(6):15–35, 2006.
47. Wang, Y., S. Zeinali-Davarani, and Y. Zhang. Arterial mechanics considering the structural and mechanical contributions of ECM constituents. *J. Biomech.* 49(12):2358–2365, 2016.
48. Cofield, R. H. Rotator cuff disease of the shoulder. *J. Bone Jt. Surg. Am.* 67(6):974–979, 1985.
49. Frandsen, J. J., N. J. Quinlan, K. M. Smith, et al. Symptomatic rotator cuff tear progression: conservatively treated full- and partial-thickness tears continue to progress. *Arthrosc. Sports Med. Rehabil.* 4(3):e1091–e1096, 2022.
50. Kim, H. M., N. Dahiya, S. A. Teefey, et al. Relationship of tear size and location to fatty degeneration of the rotator cuff. *J. Bone Jt. Surg. Am.* 92(4):829–839, 2010.
51. Moosmayer, S., G. Lund, U. S. Seljom, et al. Tendon repair compared with physiotherapy in the treatment of rotator cuff tears: a randomized controlled study in 103 cases with a five-year follow-up. *J. Bone Jt. Surg. Am.* 96(18):1504–1514, 2014.
52. Ruotolo, C., J. E. Fow, and W. M. Nottage. The supraspinatus footprint: an anatomic study of the supraspinatus insertion. *Arthroscopy*. 20(3):246–249, 2004.

53. Miller, R. M., Y. Fujimaki, D. Araki, V. Musahl, and R. E. Debski. Strain distribution due to propagation of tears in the anterior supraspinatus tendon. *J. Orthop. Res.* 32(10):1283–1289, 2014.
54. Vidt, M. E., A. C. Santago 2nd., A. P. Marsh, et al. Modeling a rotator cuff tear: individualized shoulder muscle forces influence glenohumeral joint contact force predictions. *Clin. Biomech. (Bristol, Avon).* 60:20–29, 2018.
55. Long, J. L., R. A. Ruberte Thiele, J. G. Skendzel, et al. Activation of the shoulder musculature during pendulum exercises and light activities. *J. Orthop. Sports Phys. Ther.* 40(4):230–237, 2010.
56. Reinold, M. M., K. E. Wilk, G. S. Fleisig, et al. Electromyographic analysis of the rotator cuff and deltoid musculature during common shoulder external rotation exercises. *J. Orthop. Sports Phys. Ther.* 34(7):385–394, 2004.
57. Redepenning, D. H., P. M. Ludewig, and J. M. Looft. Finite element analysis of the rotator cuff: a systematic review. *Clin. Biomech. (Bristol, Avon).* 71:73–85, 2020.
58. Matthew Miller, R., J. Thunes, V. Musahl, S. Maiti, and R. E. Debski. A validated, specimen-specific finite element model of the supraspinatus tendon mechanical environment. *J. Biomech. Eng.* 141(11):11103, 2019.
59. Matsuhashi, T., A. W. Hooke, K. D. Zhao, et al. Tensile properties of a morphologically split supraspinatus tendon. *Clin. Anat.* 27(5):702–706, 2014.
60. Sano, H., T. Hatta, N. Yamamoto, and E. Itoi. Stress distribution within rotator cuff tendons with a crescent-shaped and an L-shaped tear. *Am. J. Sports Med.* 41(10):2262–2269, 2013.
61. Hardy, P., and S. Sanghavi. Rotator cuff injury: still a clinical controversy? *Knee Surg. Sports Traumatol. Arthrosc.* 17(4):325–327, 2009.
62. Thunes, J., R. Matthew Miller, S. Pal, et al. The effect of size and location of tears in the supraspinatus tendon on potential tear propagation. *J. Biomech. Eng.* 137(8):081012, 2015.
63. Ranebo, M. C., H. C. Björnsson Hallgren, T. Holmgren, and L. E. Adolfsson. Surgery and physiotherapy were both successful in the treatment of small, acute, traumatic rotator cuff tears: a prospective randomized trial. *J. Shoulder Elbow Surg.* 29(3):459–470, 2020.
64. Holmgren, T., H. B. Hallgren, B. Oberg, L. Adolfsson, and K. Johansson. Effect of specific exercise strategy on need for surgery in patients with subacromial impingement syndrome: randomised controlled study. *Br. J. Sports Med.* 48(19):1456–1457, 2014.
65. Kuhn, J. E., W. R. Dunn, R. Sanders, et al. Effectiveness of physical therapy in treating atraumatic full-thickness rotator cuff tears: a multicenter prospective cohort study. *J. Shoulder Elbow Surg.* 22(10):1371–1379, 2013.
66. Weber, S., and J. Chahal. Management of rotator cuff injuries. *J. Am. Acad. Orthop. Surg.* 28(5):e193–e201, 2020.
67. Sellers, T. R., A. Abdelfattah, and M. A. Frankle. Massive rotator cuff tear: when to consider reverse shoulder arthroplasty. *Curr. Rev. Musculoskelet. Med.* 11(1):131–140, 2018.
68. Mall, N. A., A. S. Lee, J. Chahal, et al. An evidenced-based examination of the epidemiology and outcomes of traumatic rotator cuff tears. *Arthroscopy*. 29(2):366–376, 2013.
69. Torchia, M. T., J. A. Sefko, K. Steger-May, et al. Evaluation of survivorship of asymptomatic degenerative rotator cuff tears in patients 65 years and younger: a prospective analysis with long-term follow-up. *J. Shoulder Elbow. Surg.* 32(7):1432–1444, 2023.
70. Putera, K. H., J. Kim, S. Y. Baek, et al. Fatigue-driven compliance increase and collagen unravelling in mechanically tested anterior cruciate ligament. *Commun Biol.* 6(1):564, 2023.
71. Williamson, P., A. Mohamadi, A. J. Ramappa, J. P. DeAngelis, and A. Nazarian. Shoulder biomechanics of RC repair and instability: a systematic review of cadaveric methodology. *J. Biomech.* 82:280–290, 2019.
72. Sano, H., H. Ishii, A. Yeadon, et al. Degeneration at the insertion weakens the tensile strength of the supraspinatus tendon: a comparative mechanical and histologic study of the bone-tendon complex. *J. Orthop. Res.* 15(5):719–726, 1997.

Publisher's Note Springer Nature remains neutral with regard to jurisdictional claims in published maps and institutional affiliations.

Springer Nature or its licensor (e.g. a society or other partner) holds exclusive rights to this article under a publishing agreement with the author(s) or other rightsholder(s); author self-archiving of the accepted manuscript version of this article is solely governed by the terms of such publishing agreement and applicable law.